iScience

CellPress
OPEN ACCESS

Article

Visualization of *trans*-interactions of a protocadherin-α between processes originating from single neurons

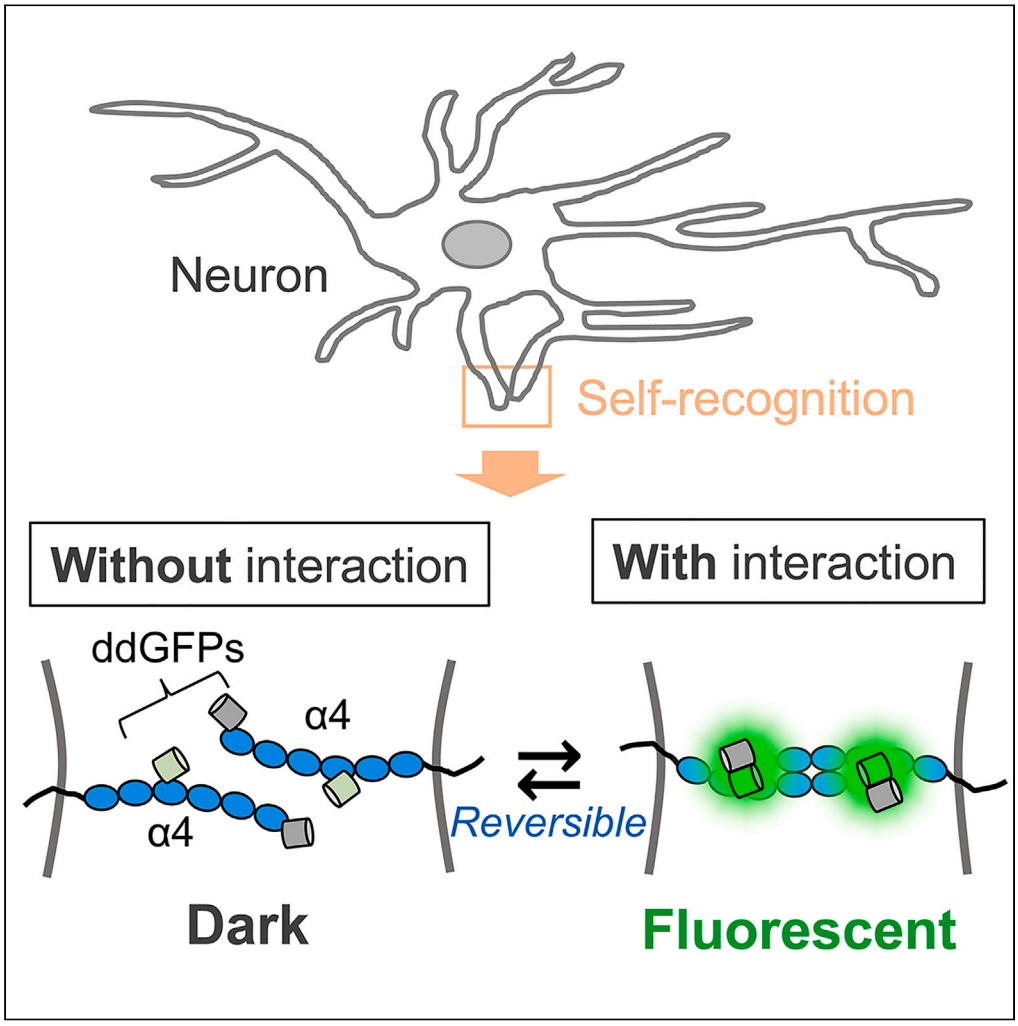

Takashi Kanadome, Natsumi Hoshino, Takeharu Nagai, Takeshi Yagi, Tomoki Matsuda

tk4@sanken.osaka-u.ac.jp (T.K.)
yagi.takeshi.fbs@osaka-u.ac.jp (T.Y.)
tmatsuda@sanken.osaka-u.ac.jp (T.M.)

Highlights

IPADs are fluorescent indicators for visualizing Pcdhα4 *trans*-interactions

IPADs can reversibly monitor Pcdhα4 *trans*-interactions

IPADs allow for visualization of self-recognition in neurons

Kanadome et al., iScience *26*, 107238
July 21, 2023
https://doi.org/10.1016/j.isci.2023.107238

iScience

CellPress
OPEN ACCESS

Article

Visualization of *trans*-interactions of a protocadherin-α between processes originating from single neurons

Takashi Kanadome,[1,2,4,5,*] Natsumi Hoshino,[3,4] Takeharu Nagai,[2] Takeshi Yagi,[3,*] and Tomoki Matsuda[2,*]

SUMMARY

Clustered protocadherin (Pcdh), a cell adhesion protein, is involved in the self-recognition and non-self-discrimination of neurons by conferring diversity on the cell surface. Although the roles of Pcdh in neurons have been elucidated, it has been challenging to visualize its adhesion activity in neurons, which is a molecular function of Pcdh. Here, we present fluorescent indicators, named IPADs, which visualize the interaction of protocadherin-α4 isoform (α4). IPADs successfully visualize not only homophilic α4 *trans*-interactions, but also combinatorial homophilic interactions between cells. The reversible nature of IPADs overcomes a drawback of the split-GFP technique and allows for monitoring the dissociation of α4 *trans*-interactions. Specially designed IPADs for self-recognition are able to monitor the formation and disruption of α4 *trans*-interactions between processes originating from the same neurons. We expect that IPADs will be useful tools for obtaining spatiotemporal information on Pcdh interactions in neuronal self-recognition and non-self-discrimination processes.

INTRODUCTION

In the brain, billions of neurons form trillions of neuronal connections.[1] To achieve proper formation of such a large number of neuronal connections, neurons are required to recognize "self" and discriminate "non-self." Self-avoidance is a process by which neurites originating from the same neurons avoid each other, preventing their own neurites from entangling with each other or creating neuronal connections on their own.[2] In vertebrates, this process is mediated in part by clustered protocadherin (Pcdh), a cell adhesion molecule. Its 58 isoforms are encoded by the *Pcdhα*, *Pcdhβ*, and *Pcdhγ* gene clusters (14*α*, 22*β*, and 22γ), which are tandemly arranged on the same chromosome.[3,4] Single-cell RT-PCR and single-cell RNA sequencing analysis have revealed that individual neurons stochastically express a different subset of Pcdh isoforms.[5–10] Pcdhs have the property of interacting only with the same isoforms, known as homophilic interactions.[11,12] In addition, Pcdhs do not interact between cells expressing even one mismatched isoform, even if they express the common isoforms, which is known as combinatorial homophilic interactions.[12] Therefore, it has been proposed that Pcdh confers identity to individual cells by providing diversity on the cell surface.[13,14]

Loss-of-function analyses of *Pcdh* genes have shown that Pcdh plays an essential role in the dendritic self-avoidance of Purkinje cells in the cerebellum and starburst amacrine cells in the retina.[15–17] In addition, Pcdh has been shown to be involved in a wide range of neuronal functions, including axonal coalescence of olfactory sensory neurons,[8,18] axonal projection of serotonergic neurons,[19–21] dendrite arborization,[22–25] synaptogenesis,[26,27] neonatal neuronal migration,[28] and neuronal survival.[29–34] While these biological roles of Pcdh have been elucidated, it is challenging to detect the cell adhesion activity in living neurons, which is a molecular function of Pcdh.

To date, the main visualization tools for detecting cell-cell contacts are fluorescent indicators using the split-GFP technique.[35,36] The split-GFP technique was originally used to detect protein-protein interactions in cells. In this technique, proteins of interest are fused to two non-fluorescent split GFP fragments. These GFP fragments associate upon protein-protein interactions and are reconstituted into a GFP molecule, resulting in fluorescence emission. Indicators based the on split-GFP technique have allowed the detection of cell-cell contacts, including neuronal connections with a single color.[37–42] However, the

[1]Precursory Research for Embryonic Science and Technology (PRESTO), Japan Science and Technology Agency (JST), Kawaguchi, Saitama 332-0012, Japan

[2]Department of Biomolecular Science and Engineering, SANKEN (The Institute of Scientific and Industrial Research), Osaka University, 8-1 Mihogaoka, Ibaraki 567-0047, Japan

[3]KOKORO-Biology Group, Graduate School of Frontier Biosciences, Osaka University, Suita 565-0871, Japan

[4]These authors contributed equally

[5]Lead contact

*Correspondence: tk4@sanken.osaka-u.ac.jp (T.K.), yagi.takeshi.fbs@osaka-u.ac.jp (T.Y.), tmatsuda@sanken.osaka-u.ac.jp (T.M.)

https://doi.org/10.1016/j.isci.2023.107238

split-GFP technique is irreversible and therefore does not allow the dissociation of cell-cell contacts to be monitored.

Recently, we developed INCIDER, which visualizes the association and dissociation of N-cadherin interactions between cells with a single color by using the dimerization-dependent green fluorescent protein (ddGFP).[43] ddGFP consists of two components, ddGFP-A and ddFP-B, which has and lacks a chromophore, respectively. ddGFP-A is quenched in the monomeric state, although it gives green fluorescence upon heterodimerization with ddFP-B.[44,45] The ddGFP technique has made it possible to monitor the dissociation of cell-cell contacts which is not possible with the split-GFP technique.

In this study, we used the ddGFP technique to develop IPADs (Indicators for Protocadherin Alpha 4 interactions upon Dimerization), indicators for visualizing *trans*-interactions of protocadherin-α4 (α4), a Pcdh isoform that we first identified as cadherin-related neural receptor 1 (CNR1).[3] IPADs successfully visualized not only homophilic α4 *trans*-interactions, but also combinatorial homophilic interactions. IPADs were also able to monitor the dissociation of α4 *trans*-interactions between cells, in contrast to the indicator based on the split-GFP technique. Using IPADs in neurons, we successfully visualized α4 *trans*-interactions between neurons. Furthermore, the formation and disruption of α4 *trans*-interactions between processes originating from single neurons were visualized using specially designed IPADs.

RESULTS

Insertion of fluorescent proteins into α4 for the development of ddGFP-based α4 indicators

First, many Pcdh constructs are introduced in this study. Their schematics are summarized in Figure S9 for ease of understanding.

To develop ddGFP-based α4 indicators for monitoring α4 *trans*-interactions between cells, we first had to determine the insertion sites of ddGFP into α4. Pcdhα isoforms, including α4, require *cis*-dimer formation with Pcdhβ or Pcdhγ isoforms as carrier proteins to localize to the plasma membrane.[12,46,47] This property makes it difficult to examine the insertion sites. A previous study showed that chimeric α4 whose EC6 domain swapped by that of a Pcdhγ isoform is able to reach the plasma membrane without carrier proteins, which inspired us to use chimeric α4 whose C-terminal region after the EC6 domain is swapped by that of PcdhγB2 (γB2). It has been reported that deletion of an intracellular domain (ICD) of Pcdhγ efficiently localizes Pcdhγ to the plasma membrane.[12,48] Although the role of an ICD of Pcdhα in its localization has not been characterized, we deleted an ICD of chimeric α4. We firstly examined the localization of C-terminally Venus-fused γB2ΔICD, α4ΔICD, and chimeric α4ΔICD (γB2ΔICD-V, α4ΔICD-V, and α4γB2EC6ΔICD-V, respectively) (Figure S1A). While α4γB2EC6ΔICD-V efficiently localized to the plasma membrane like γB2ΔICD-V, α4ΔICD-V failed to localize to the plasma membrane (Figure S1B).

We have previously developed FRET-based γB2 indicators that mTurquoise2 and Venus are inserted into the EC1 and EC5 domains as FRET donor and acceptor fluorescent proteins, respectively.[49] To determine the insertion sites of fluorescent proteins into α4γB2EC6ΔICD, we referred to those sites of FRET-based γB2 indicators and prepared α4γB2EC6ΔICD constructs in which Venus is inserted into corresponding sites of FRET-based γB2 indicators (α4γB2EC6ΔICD-EC1-V and α4γB2EC6ΔICD-EC5-V) (Figure S1C). However, they hardly localized at the plasma membrane (Figure S1D). Next, we tried to insert Venus based on a crystal structure of a *trans*-dimer consisting of EC1-EC4 domains of α4 (PDB: 5DZW).[50] We expected that the N-terminus in EC1 of one α4 molecule and the loop between the βC and βD strands in EC4 of another α4 molecule would be close to each other, forming a *trans*-dimer. Based on this expectation, we inserted Venus individually into these regions of chimeric α4ΔICD (V-α4γB2EC6ΔICD and α4γB2EC6ΔICD-EC4-V) (Figure S1C). Both constructs were clearly localized to the plasma membrane (Figure S1D). We selected these sites as candidate ddGFP insertion sites. Next, we applied these chimeric α4 insertion sites to the original α4 (Figure 1A). We prepared Venus-inserted α4ΔICDs (V-α4ΔICD and α4ΔICD-EC4-V) and compared their localization with α4ΔICD-V as a positive control (Figure 1B). Similar to α4ΔICD-V, both Venus-inserted α4ΔICDs reached the plasma membrane in the presence of a carrier protein (C-terminally mCherry-fused γB2, γB2ΔICD-mCh), whereas they mainly localized to intracellular spaces in the absence of a carrier protein (Figure 1C). To examine the effect of Venus-insertion on the adhesive function of α4, we performed a cell aggregation assay using K562 cells. K562 cells lack endogenous cell adhesion proteins and have been used to analyze the adhesive functions of exogenous cell adhesion proteins.[11,12,51] We used C-terminally mCherry-fused γB2ΔICD lacking an EC1 domain (γB2ΔEC1ΔICD-mCh) as a carrier

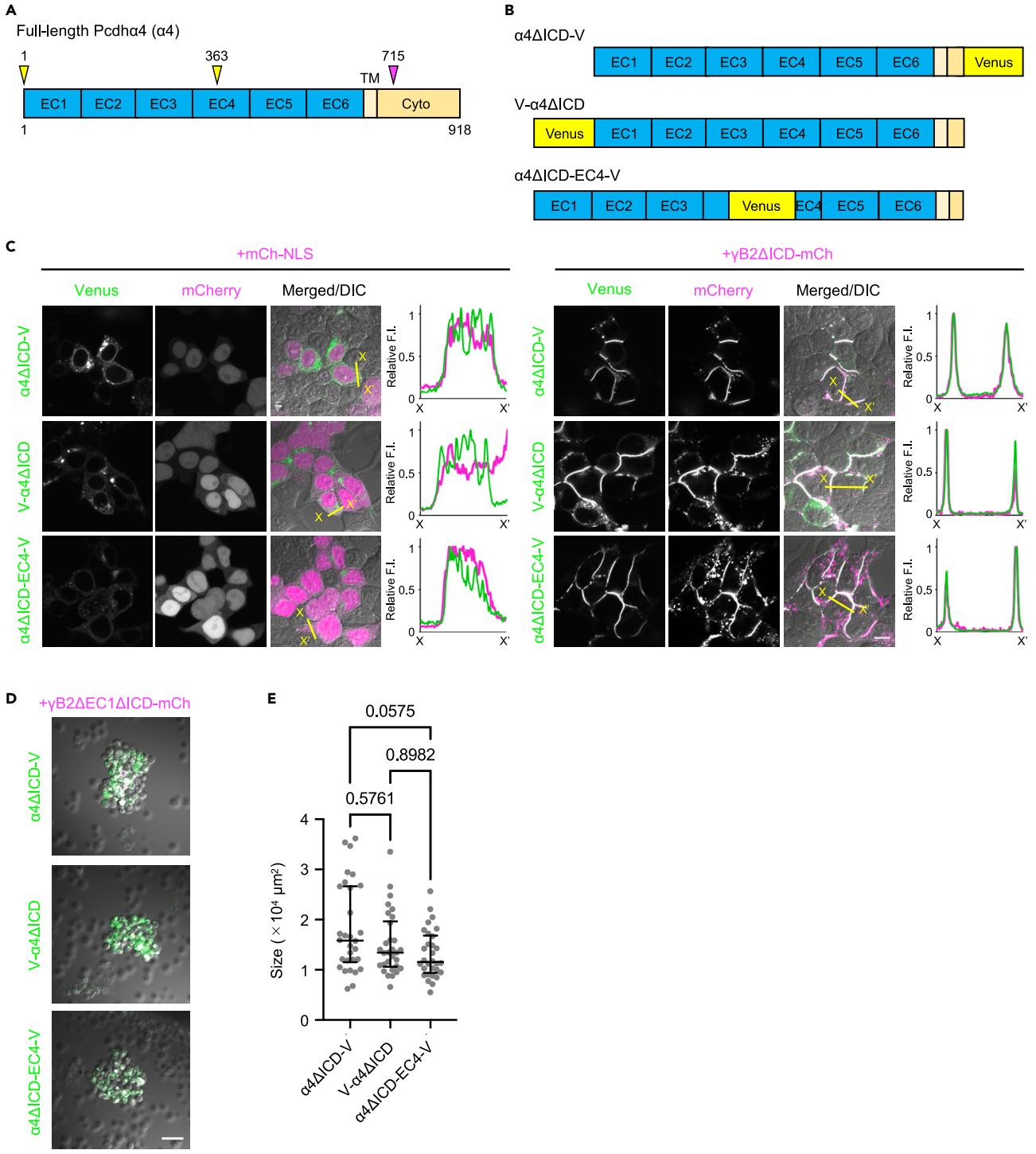

Figure 1. Molecular design and characterization of Venus-inserted α4

(A) Schematic representation of full-length protocadherin-α4 (α4). α4 is drawn as serially repeated extracellular domains (EC domains), a transmembrane region (TM), and a cytoplasmic region (Cyto). The insertion positions (amino acid position 1st and 363rd residues in the mature form) of Venus and an initiation position of an intracellular domain (ICD) are indicated by yellow and magenta arrowheads, respectively.

(B) Schematics of Venus-fused or -inserted α4ΔICD. ΔICD indicates deletion of an intracellular domain (ICD).

(C) Localization of Venus-inserted α4ΔICDs in HEK293T cells. HEK293T cells transiently expressing α4 constructs with mCherry-fused NLS (mCh-NLS) or mCherry-fused protocadherin-γB2 lacking an ICD (γB2ΔICD-mCh) as a carrier protein were observed using a confocal microscope. Scale bar, 20 μm.

Figure 1. *Continued*

Fluorescence profiles along the yellow lines from X to X′ are shown on the right. Relative fluorescence intensities of Venus and mCherry are represented by green and magenta lines, respectively. In all conditions, 14 fields of view were observed from two independent experiments.

(D) Effect of Venus insertion on the adhesive function. K562 cells expressing the indicated α4 constructs with mCherry-fused γB2 lacking an EC1 domain and an ICD (γB2ΔEC1ΔICD-mCh) were cultured and observed using a confocal microscope. Scale bar, 50 μm.

(E) The size of the formed cell aggregates was measured and compared. Results are presented as lower quartile (lower whisker), median (center line), and upper quartile (upper whisker). Significant differences were analyzed by Kruskal-Wallis test, followed by Dunn's multiple comparison test. p values are shown in the graph. 30 cell aggregates were analyzed in each sample from three independent experiments.

protein that cannot form a *trans*-dimer, but can function as a carrier protein to evaluate only the adhesive function of α4 constructs.[12] We were able to observe cell aggregates by co-expression of α4 constructs with a carrier protein (Figure 1D). V-α4ΔICD and α4ΔICD-EC4-V tended to show slightly smaller cell aggregates than α4ΔICD-V, although significant differences were not confirmed (Figure 1E). These results indicate that the insertion of Venus into the EC1 and EC4 domains of α4 does not significantly affect the localization and adhesive function of α4.

Development of separate type ddGFP-based α4 indicators (sIPADs)

By replacing Venus with ddGFP-A and ddFP-B in α4ΔICD-EC4-V and V-α4ΔICD, respectively, we generated ddGFP-A-inserted α4ΔICD (α4ΔICD-EC4-GA) and ddFP-B-inserted α4ΔICD (B-α4ΔICD) (Figure 2A). We used two variants of ddFP-B with different affinities to ddGFP-A, ddFP-B1 and ddFP-B3 (K_d = 3 μM and 40 μM, respectively).[45] The indicators consisting of the combinations of α4ΔICD-EC4-GA/B1-α4ΔICD and α4ΔICD-EC4-GA/B3-α4ΔICD were designated sIPAD (separate type Indicator for Protocadherin-Alpha 4 interaction upon Dimerization)-1 and sIPAD-3, respectively. To investigate the detectability of sIPADs in α4 *trans*-interactions between cells, we co-cultured HEK293T cells expressing only one of the sIPAD components. C-terminally EBFP2- and mCherry-fused γB2ΔEC1ΔICD (γB2ΔEC1ΔICD-EB and γB2ΔEC1ΔICD-mCh) as carrier proteins were co-expressed with α4ΔICD-EC4-GA and B-α4ΔICD, respectively. Fluorescence was observed at the cell adhesion sites between EBFP2- and mCherry-positive cells, confirming the detection of α4 *trans*-interactions by sIPADs (Figure 2B). The fluorescence intensity was comparable between sIPAD-1 and sIPAD-3 (Figure 2C). It is possible that heterodimerization between ddGFP-A and ddFP-B enhances the association of cell-cell interactions. To address this possibility, we compared the adhesive function between Venus-inserted α4s and sIPADs by a cell aggregation assay using K562 cells (Figure 2D). Although cell aggregates of sIPAD-1 were significantly smaller than those of Venus constructs and sIPAD-3, their differences were not so large (Figure 2E). This result suggests that heterodimerization between ddGFP-A and ddFP-Bs does not enhance cell-cell interactions.

Visualization of the α4 homophilic interactions

To investigate whether sIPADs visualize α4 homophilic interactions, we prepared ddGFP-based indicators for protocadherin-α8 (α8), one of the closely related isoforms of α4. We firstly confirmed their homophilic interactions using C-terminally Venus-fused α4ΔICD and α8ΔICD (α4ΔICD-V and α8ΔICD-V). Cell aggregation assay using K562 cells showed that α4ΔICD-V interacted with α4ΔICD-V, but not with α8ΔICD-V, and vice versa (Figure S2A). We also investigated whether ddGFP constructs homophilically interact. Cells expressing the same Pcdhα isoform formed cell aggregates with cells expressing the same Pcdhα isoform, but not with cells expressing the different Pcdhα isoform (Figure S2B). Co-culture experiments using HEK293T cells individually expressing sIPAD components showed that fluorescence was generated by cell mixtures expressing the same Pcdhα isoforms, but not different isoforms (Figures 3A and 3B). These results suggest that sIPADs visualize α4 homophilic interactions.

Detectability of combinatorially expressed α4 interactions

A cell aggregation assay from a previous study showed that only cells expressing identical Pcdh isoforms co-aggregated, whereas cells co-expressing different combinations of Pcdh isoforms did not co-aggregate, even if they expressed the partially shared isoforms.[12] We firstly confirmed whether K562 cells co-expressing α4ΔICD-V with different carrier proteins could co-aggregate. Cells co-expressing α4ΔICD-V with C-terminally EBFP2-fused γB2ΔICD (γB2ΔICD-EB) co-aggregated with cells co-expressing α4ΔICD-V with C-terminally mCherry-fused γB2ΔICD (γB2ΔICD-mCh), although they did not co-aggregate with cells co-expressing α4ΔICD-V with C-terminally mCherry-fused γA3ΔICD (γA3ΔICD-mCh) (Figure S3A). Similar to these results, cells co-expressing ddGFP-A-inserted α4ΔICD (α4ΔICD-EC4-GA) with γB2ΔICD-EB formed

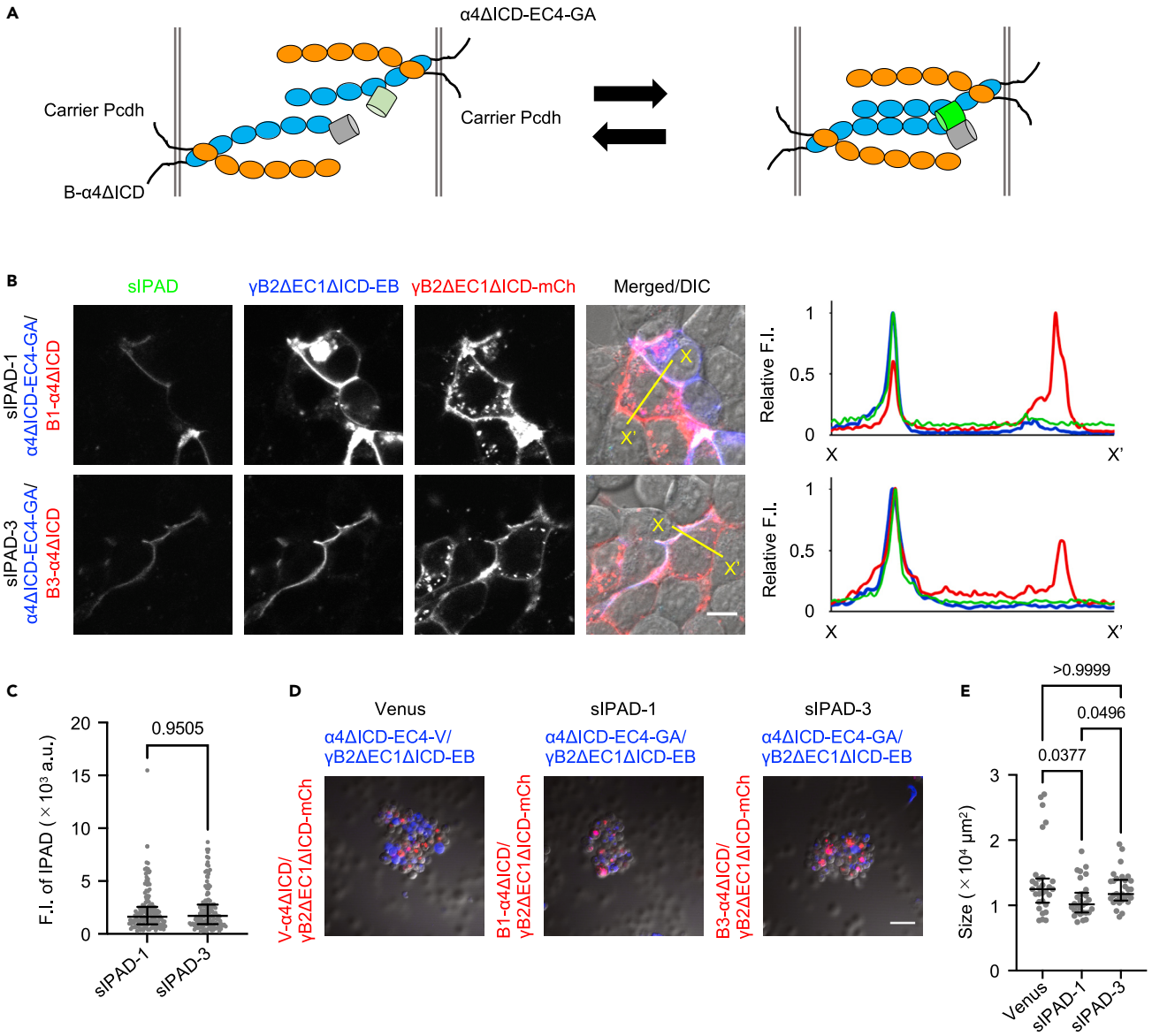

Figure 2. Design of ddGFP-based indicators for visualization of α4 *trans*-interactions

(A) Schematics of α4 interactions by sIPAD. α4 is represented by six serially repeated extracellular EC domains. ddGFP-A and ddFP-Bs are shown as green and gray cylinders, respectively. Binding of α4ΔICD-EC4-GA to B-α4ΔICD causes ddGFP-A and ddFP-B to form a heterodimer, resulting in green fluorescence.

(B) Fluorescence and DIC images of α4 *trans*-interactions between cells. HEK293T cells individually expressing sIPAD components, i.e., α4ΔICD-EC4-GA and B-α4ΔICD (B1-α4ΔICD or B3-α4ΔICD), were co-cultured, and then observed using a confocal microscope. EBFP2- or mCherry-fused γB2ΔEC1ΔICD (γB2ΔEC1ΔICD-EB and γB2ΔEC1ΔICD-mCh) were co-expressed with α4ΔICD-EC4-GA and B-α4ΔICD as carrier proteins. Scale bar, 20 μm. Fluorescence profiles along the yellow lines from X to X′ are shown on the right. Relative fluorescence intensities of sIPAD, EBFP2, and mCherry are represented by green, blue, and red lines, respectively.

(C) Fluorescence intensity of sIPAD at the cell adhesion sites was quantified and compared between sIPAD-1 and sIPAD-3. Results are presented as lower quartile (lower whisker), median (center line), and upper quartile (upper whisker). A significant difference was analyzed by Kolmogorov-Smirnov test. A p value is shown in the graph. 148 (sIPAD-1) and 135 (sIPAD-3) cell adhesion sites from two independent experiments were analyzed.

(D) Effect of ddFPs insertion on the adhesive function. K562 cells transiently expressing the indicated constructs were co-cultured and observed using a confocal microscope. Scale bar, 50 μm.

(E) The size of formed cell aggregates was measured and compared. Results are presented as lower quartile (lower whisker), median (center line), and upper quartile (upper whisker). Significant differences were analyzed by Kruskal-Wallis test, followed by Dunn's multiple comparison test. p values are shown in the graph. 30 cell aggregates were analyzed in each sample from three independent experiments.

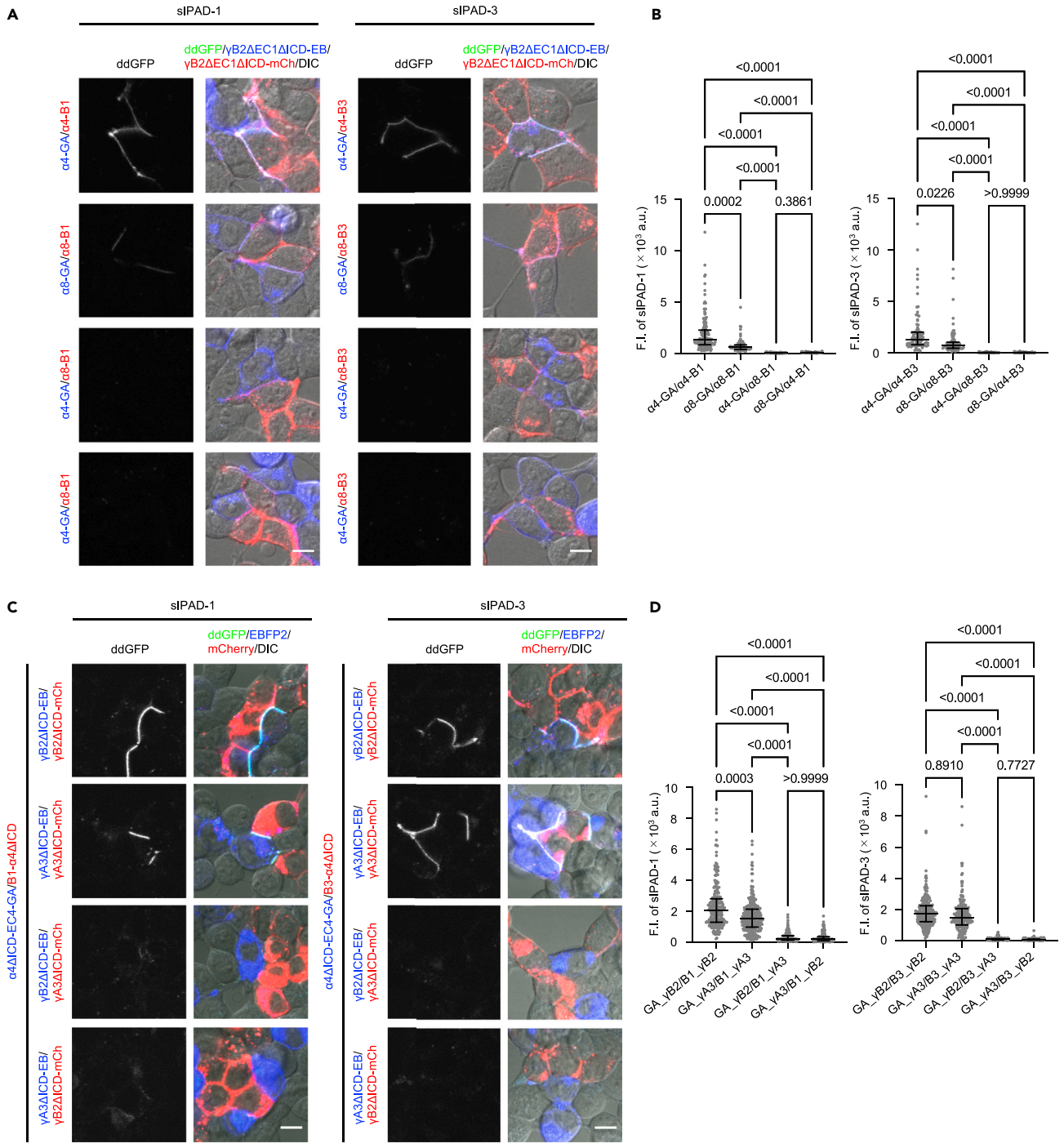

Figure 3. Specificity of sIPAD

(A) Visualization of homophilic α4 interactions by sIPAD. HEK293T cells individually expressing ddFP-inserted α4ΔICD or α8ΔICD constructs with carrier proteins were co-cultured in the indicated combination and observed using a confocal microscope. Scale bar, 10 μm.

(B) Fluorescence intensity of sIPAD at the cell adhesion sites was quantified and compared. Data are presented as lower quartile (lower whisker), median (center line), and upper quartile (upper whisker). Significant differences were analyzed by Kruskal-Wallis test, followed by Dunn's multiple comparison test. *p* values are shown in the graphs. 140 (α4-GA/α4-B1), 78 (α8-GA/α8-B1), 76 (α4-GA/α8-B1), 83 (α8-GA/α4-B1), 87 (α4-GA/α4-B3), 71 (α8-GA/α8-B3), 45 (α4-GA/α8-B3), and 63 (α8-GA/α4-B3) cell adhesion sites from two independent experiments were analyzed.

(C) Visualization of combinatorially expressed α4 interaction. HEK293T cells individually expressing sIPAD components with different carrier proteins (γB2 or γA3) were co-cultured in the indicated combination and observed using a confocal microscope. Scale 10 μm.

Figure 3. *Continued*

(D) Fluorescence intensity of sIPAD at the cell adhesion sites was quantified and compared. Data are presented as lower quartile (lower whisker), median (center line), and upper quartile (upper whisker). Significant differences were analyzed by Kruskal-Wallis test, followed by Dunn's multiple comparison test. p values are shown in the graphs. 247 (GA_γB2/B1_γB2), 287 (GA_γA3/B1_γA3), 188 (GA_γB2/B1_γA3), 200 (GA_γA3/B1_γB2), 213 (GA_γB2/B3_γB2), 210 (GA_γA3/B3_γA3), 177 (GA_γB2/B3_γA3), and 212 (GA_γA3/B3_γB2) cell adhesion sites from three independent experiments were analyzed.

co-aggregation with those co-expressing ddFP-B-inserted α4ΔICD (B-α4ΔICD) with γB2ΔICD-mCh, but not γA3ΔICD-mCh (Figure S3B). We next examined the effect of combinatorial expression on sIPAD fluorescence in HEK293T cells. When the same Pcdh isoforms (γB2 or γA3) were used as carrier proteins, sIPADs showed fluorescence. In contrast, fluorescence was dramatically decreased at the cell adhesion sites formed by cells expressing different carrier proteins (Figures 3C and 3D). These results suggest that sIPADs successfully reflect homophilic interactions of combinatorially expressed Pcdhs.

Comparison between sIPAD and split-GFP technique

To compare the relative performance between sIPADs and the split-GFP technique, we newly prepared a split-GFP technique-based α4 indicator by replacing ddGFP-A and ddFP-B in sIPADs with the N-terminal fragment (sfGFP1-7, sfGN) and the C-terminal fragment of superfolder GFP (sfGFP8-11, sfGC), respectively.[41,42] The split-GFP technique-based α4 indicator showed fluorescence at the cell adhesion sites similar to sIPADs, and its fluorescence intensity was more than twice as high as that of sIPADs (Figures 4A and 4B). Reconstitution of the split-GFP fragments is irreversible, thereby split-GFP-system based α4 indicator is potentially unable to monitor the dissociation of cell-cell interactions. To evaluate the relative dissociation property, we examined the effect of EGTA treatment on pre-formed cell-cell contacts. We first co-cultured HEK293T cells individually expressing sIPADs or the split-GFP technique-based α4 indicator components for 6 h, and then further cultured them in the presence or absence of 10 mM EGTA for 2 h. The fluorescence intensity of sIPADs was dramatically decreased by incubation with EGTA, while the split-GFP technique-based α4 indicator showed signals regardless of EGTA treatment (Figures 4C and 4D). This result shows that sIPADs successfully monitor the dissociation of α4 *trans*-interactions between cells unlike the split-GFP technique-based α4 indicator.

Development and characterization of combined IPADs (cIPADs)

Crystal structures of Pcdh *trans*-dimers clearly indicate that Pcdh forms a *trans*-dimer with a head-to-tail orientation unlike classical cadherins that form a head-to-head interacting interface.[50] This head-to-tail interacting interface allows the development of combined IPADs (cIPADs) (Figure 5A). Based on this idea, we constructed α4 indicators that ddGFP-A and ddFP-B are inserted into a single α4 molecule. We firstly investigated the adhesive function of cIPADs. Cell aggregation assay using K562 cells showed that both had an adhesive function, although that of cIPAD-1 was lower than that of cIPAD-3 (Figures 5B and 5C). cIPADs showed fluorescence at the cell adhesion sites in the presence of a carrier protein (γB2ΔEC1ΔICD-mCh), although fluorescence was hardly observed at the cell adhesion sites when mCherry tagged with a nuclear localization signal (mCh-NLS) was co-expressed (Figures 5D and 5E). It is possible that intramolecular heterodimerization of ddGFP or intermolecular heterodimerization of ddGFP between cIPADs on the same membrane occurs through cell-cell contacts. To investigate this possibility, we performed a co-culture experiment between cells expressing cIPADs and cells expressing α4ΔICD lacking a fluorescent protein (α4ΔICD). C-terminally mCherry-fused and EBFP2-fused γB2ΔEC1ΔICD (γB2ΔEC1ΔICD-mCh and γB2ΔEC1ΔICD-EB) were co-expressed with cIPAD and α4ΔICD as carrier proteins, respectively. If fluorescence is detected between EBFP2-positive and mCherry-positive cells (B-R), it indicates that cIPADs fluoresce with the previous possibility. On the other hand, if fluorescence is detected only between mCherry-positive cells (R-R), the fluorescence of cIPADs would be solely due to α4 *trans*-interactions. α4ΔICD-V showed fluorescence not only at R-R (Figure 5G, open arrowheads), but also at B-R (Figure 5G, closed arrowheads). In contrast, cIPADs fluorescence was observed at R-R (Figure 5G, open arrowheads), but not at B-R (Figure 5G, closed arrowheads). While α4ΔICD-V showed a low contrast of Venus signals between R-R and B-R (1.54), those of cIPAD-1 and -3 signals between R-R and B-R were high (7.42 and 14.9, respectively) (Figure 5H). These results indicate that cIPADs predominantly visualize α4 *trans*-interactions.

α4 *trans*-interactions in neurons visualized by IPAD

We examined the detectability of IPADs in neurons. We individually expressed full-length sIPAD-3 components with γB2ΔEC1ΔICD-EB or γB2ΔEC1ΔICD-mCh in dissociated hippocampal neurons and co-cultured them. sIPAD fluorescence was detected at the contact sites of neuronal processes (Figures 6A and S4A).

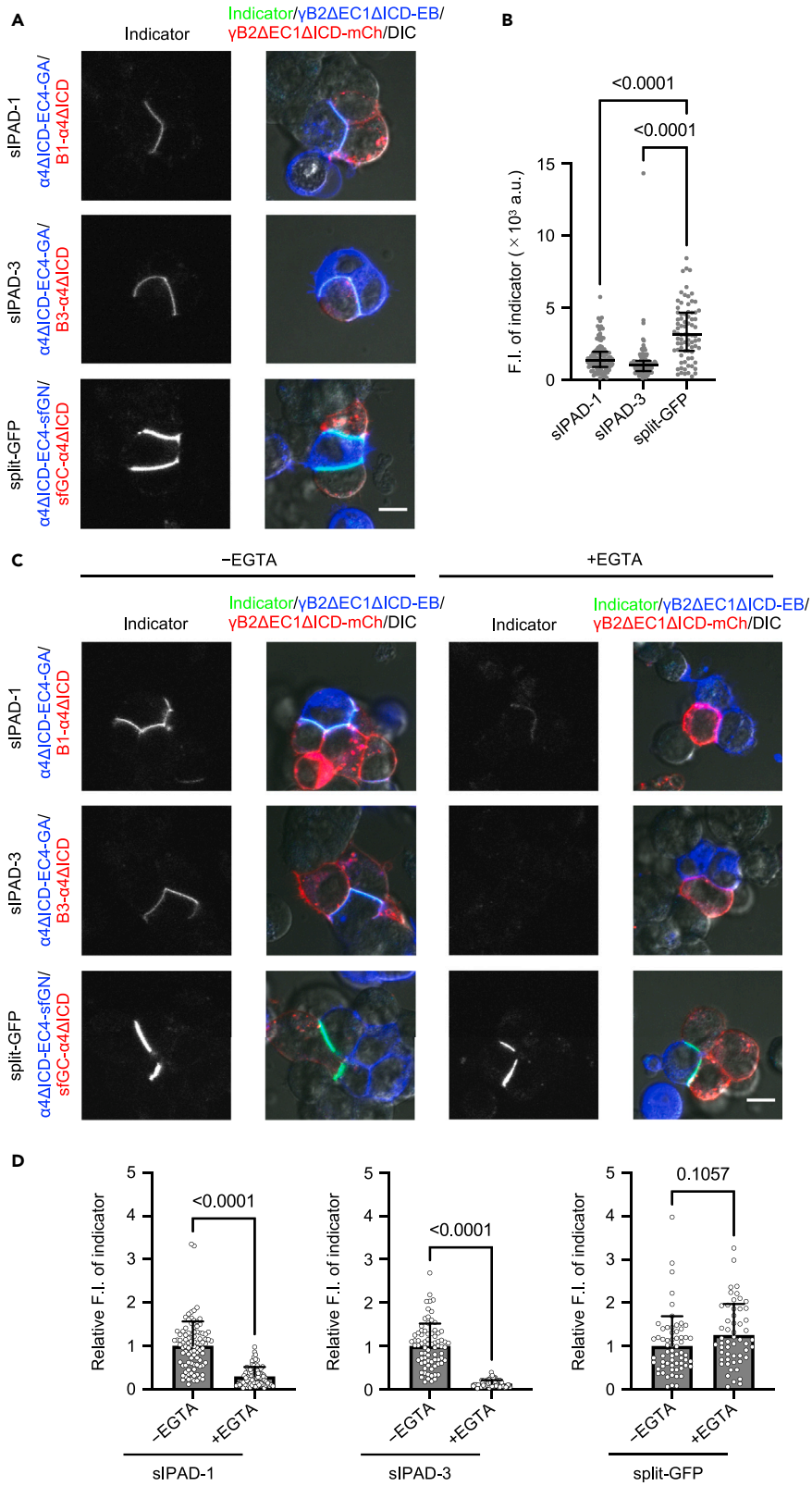
A
Indicator
Indicator/γB2ΔEC1ΔICD-EB/
γB2ΔEC1ΔICD-mCh/DIC
sIPAD-1
α4ΔICD-EC4-GA/
B1-α4ΔICD
sIPAD-3
α4ΔICD-EC4-GA/
B3-α4ΔICD
split-GFP
α4ΔICD-EC4-sfGN/
sfGC-α4ΔICD
B
<0.0001
<0.0001
F.I. of indicator (×10³ a.u.)
15
10
5
0
sIPAD-1
sIPAD-3
split-GFP
C
−EGTA
+EGTA
Indicator
Indicator/γB2ΔEC1ΔICD-EB/
γB2ΔEC1ΔICD-mCh/DIC
sIPAD-1
α4ΔICD-EC4-GA/
B1-α4ΔICD
sIPAD-3
α4ΔICD-EC4-GA/
B3-α4ΔICD
split-GFP
α4ΔICD-EC4-sfGN/
sfGC-α4ΔICD
D
Relative F.I. of indicator
<0.0001
<0.0001
0.1057
−EGTA
+EGTA
sIPAD-1
sIPAD-3
split-GFP

Figure 4. Comparison between sIPAD and split-GFP technique

(A) Comparison of brightness between sIPAD and split-GFP technique. HEK293T cells individually expressing the indicated components with carrier proteins were co-cultured and observed using a confocal microscope. Scale bar, 10 μm.

(B) Fluorescence intensity of the indicators at the cell adhesion sites was quantified. Data are presented as lower quartile (lower whisker), median (center line), and upper quartile (upper whisker). Significant differences were analyzed by Kruskal-Wallis test, followed by Dunn's multiple comparison test. p values are shown in the graph. 107 (sIPAD-1), 106 (sIPAD-3), and 79 (split-GFP) cell adhesion sites from three independent experiments were analyzed.

(C) Comparison of reversibility between sIPAD and split-GFP. HEK293T cells individually expressing the indicated components with carrier proteins were co-cultured for 6 h, and then co-cultured in the presence or absence of 10 mM EGTA for further 2 h. Scale bar, 10 μm.

(D) Fluorescence intensity of the indicators at the cell-cell contact sites in the presence or absence of 10 mM EGTA was quantified and normalized by the mean values in the absence of 10 mM EGTA. Data are presented as relative mean values ± SD. Significant differences were analyzed by Kolmogorov-Smirnov test. p values are shown in the graphs. 94 (-EGTA, sIPAD-1), 84 (+EGTA, sIPAD-1), 78 (-EGTA, sIPAD-3), 69 (+EGTA, sIPAD-3), 63 (-EGTA, split-GFP), 54 (+EGTA, split-GFP) cell–cell contact sites from three independent experiments were analyzed.

The signal was specifically detected between neuronal processes of an α4-EC4-GA-expressing neuron and a B3-α4-expressing neuron. In contrast, a process of an α4-EC4-GA-expressing neuron that was not in contact with a B3-α4-expressing neuron showed little fluorescence (Figures 6B and S4B). sIPAD-1 was also able to visualize α4 *trans*-interactions between processes (Figure S5).

We next applied cIPADs to neurons. cIPADs could potentially visualize process-process interactions derived from the same neurons. As expected, cIPAD-3 fluorescence was detected at process-process contact regions on the same neuron, but not at free processes. (Figures 6C, 6D, and S6). α4 *trans*-interactions on processes between different neurons were also visualized by cIPAD-3 (Figure S7). Similar to cIPAD-3, cIPAD-1 visualized α4 *trans*-interactions at process-process contact regions on the same cell (Figure S8). We finally examined the dynamics of α4 *trans*-interactions between processes from the same neuron. We observed dissociated hippocampal neurons expressing cIPAD-3 (Figure 6E). Time-lapse imaging of α4 *trans*-interactions visualized by cIPAD-3 on processes at the white square region in Figure 6E was performed. We successfully observed the formation of α4 *trans*-interactions after process-process contact and its disruption after dissociation of process-process contact (Figure 6F). These results suggest that IPADs are applicable to neurons and can monitor the formation and disruption of α4 *trans*-interactions.

DISCUSSION

Here, we developed ddGFP-based indicators for visualization of α4 *trans*-interactions by inserting ddGFP-A and ddFP-B into α4. We used ddFP-B1 and ddFP-B3 to prepare ddFP-B-inserted α4. The K_d of ddFP-B1 and ddFP-B3 to ddGFP-A is approximately 3 μM and 40 μM, respectively.[45] On the other hand, the K_d of a *trans*-dimer formed by α4 EC1-EC4 domains is approximately 38 nM.[50] Since the affinity of α4 *trans*-interactions is much higher than that of ddGFP-AB1 and ddGFP-AB3, both do not appear to have a significant effect on α4 *trans*-interactions. The fluorescence intensity of sIPAD-1 and sIPAD-3 was comparable (Figure 2C). However, sIPAD-1 had fluorescence, although significantly lower, in a co-culture experiment using different carrier proteins (Figures 3C and 3D) and in an EGTA-treated experiment (Figures 4C and 4D). These results suggest that sIPAD-1 may give rise to a background signal even under conditions where α4 does not form *trans*-interactions. In contrast, the same situation for sIPAD-1 was not confirmed for sIPAD-3. Therefore, it is possible that IPAD-3 is more suitable than IPAD-1 for accurate visualization of α4 *trans*-interactions.

To investigate the specificity of sIPADs, an α8 indicator was generated based on the same procedure used to develop sIPADs. The α8 indicator was able to detect α8 *trans*-interactions in HEK293T cells, but its fluorescence was significantly lower than that of sIPADs (Figures 3A and 3B). In addition, cell aggregation assay using K562 cells showed that ddGFP-inserted α8 tended to result in much smaller cell aggregation than C-terminally Venus-fused α8 (Figures S2A and S2B). One possible reason for these results is that the insertion of ddGFP into α8 may have reduced adhesive functions and localization to the plasma membrane. While it is possible to develop other Pcdhs indicators by inserting ddGFP into the corresponding sites, as in α8, it would be necessary to optimize the insertion sites according to each Pcdh isoform to solve the previous problems.

Unlike IPAD, the split-GFP technique-based α4 indicator is irreversible and therefore cannot monitor the dissociation of cell-cell interactions. However, the indicator also has the following advantages. The

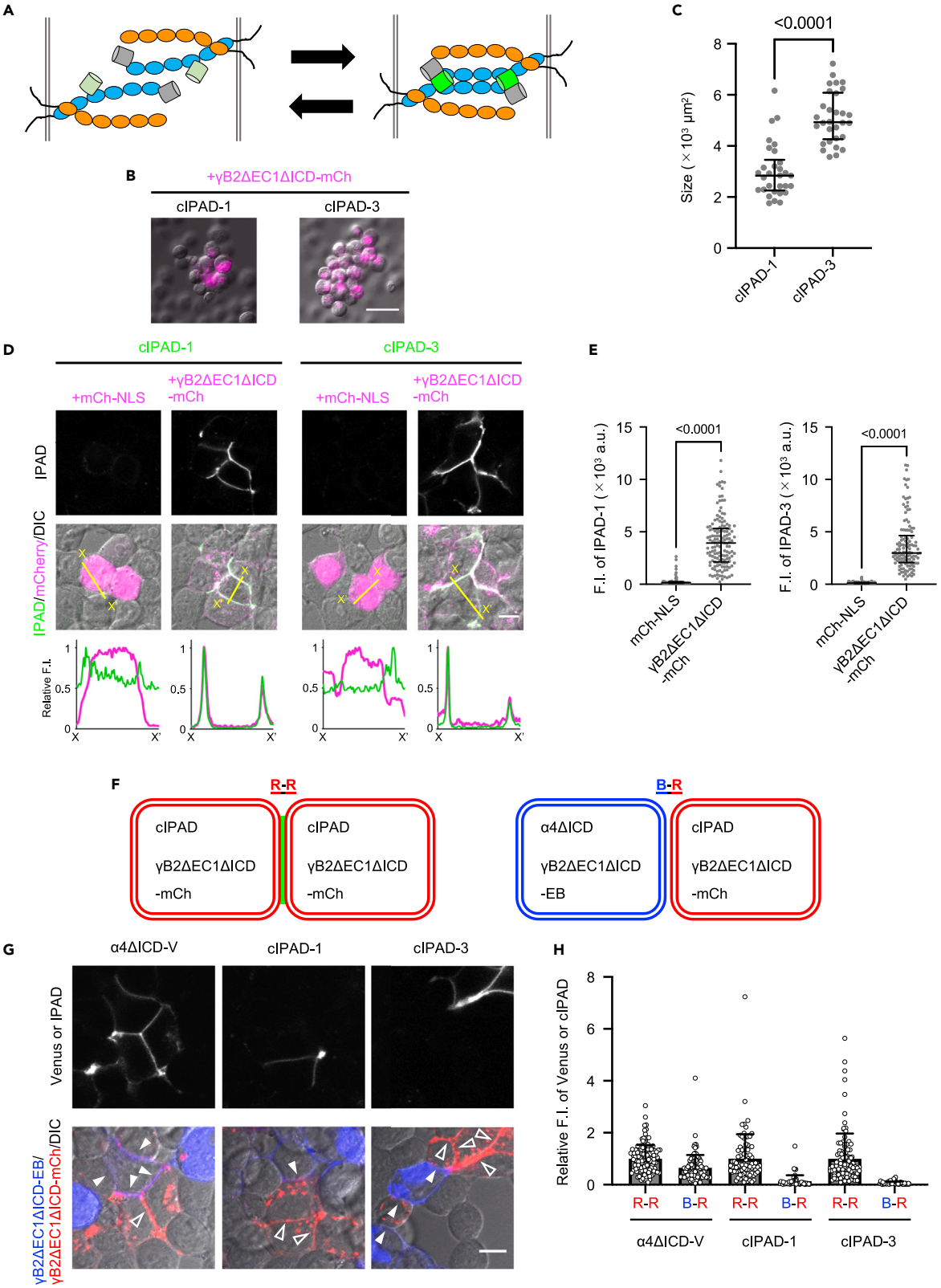
A
B
+γB2ΔEC1ΔICD-mCh
cIPAD-1
cIPAD-3
C
<0.0001
Size (×10³ μm²)
cIPAD-1
cIPAD-3
D
cIPAD-1
cIPAD-3
+mCh-NLS
+γB2ΔEC1ΔICD -mCh
IPAD
IPAD/mCherry/DIC
Relative F.I.
E
F.I. of IPAD-1 (×10³ a.u.)
F.I. of IPAD-3 (×10³ a.u.)
<0.0001
mCh-NLS
γB2ΔEC1ΔICD -mCh
F
R-R
B-R
cIPAD
γB2ΔEC1ΔICD -mCh
α4ΔICD
γB2ΔEC1ΔICD -EB
G
α4ΔICD-V
cIPAD-1
cIPAD-3
Venus or IPAD
γB2ΔEC1ΔICD-EB/
γB2ΔEC1ΔICD-mCh/DIC
H
Relative F.I. of Venus or cIPAD
R-R
B-R
α4ΔICD-V
cIPAD-1
cIPAD-3

Figure 5. Evaluation of cIPAD

(A) Schematics of α4 *trans*-interactions visualized by cIPAD.

(B) Adhesive function of cIPAD. K562 cells expressing cIPAD with γB2ΔEC1ΔICD-mCh as a carrier protein were cultured and observed using a confocal microscope. Scale bar, 40 μm.

(C) The size of the formed cell aggregates was measured and compared. Results are presented as lower quartile (lower whisker), median (center line), and upper quartile (upper whisker). A significant difference was analyzed by Kolmogorov-Smirnov test. A p value is shown in the graph. 30 cell aggregates were analyzed in each sample from three independent experiments.

(D) Visualization of α4 *trans*-interactions between cells by cIPAD. HEK293T cells expressing cIPAD with mCherry-fused NLS (mCh-NLS) or γB2ΔEC1ΔICD-mCh were observed. Scale 10 μm. Fluorescence profiles along the yellow lines from X to X′ are shown at the bottom. Relative fluorescence intensities of cIPAD and mCherry are represented by green and magenta lines, respectively. (E) Fluorescence intensity of cIPAD at the cell adhesion sites was quantified. Significant differences were analyzed by Kolmogorov-Smirnov test. p values are shown in the graphs. 65 (+mCh-NLS, cIPAD-1), 144 (+γB2ΔEC1ΔICD-mCh, cIPAD-1), 99 (+mCh-NLS, cIPAD-3), and 126 (+γB2ΔEC1ΔICD-mCh, cIPAD-3) cell adhesion sites from two independent experiments were analyzed.

(F) Schematic representation of the co-culture experiment between cells expressing cIPAD and cells expressing α4ΔICD, not cIPAD.

(G) HEK293T cells expressing the indicated constructs were co-cultured and observed using a confocal microscope. Cell adhesion sites between red cells and between blue cells and red cells are described as R-R and B-R, respectively. Closed and open arrowheads indicate cell adhesion sites between mCherry-positive cells/EBFP2-positive cells (B-R) and mCherry-positive cells (R-R), respectively. Scale bar, 10 μm. (H) Fluorescence intensity of Venus and cIPAD at R-R and B-R cell adhesion sites were quantified and normalized by the mean values of R-R cell adhesion sites. Data are presented as relative mean values ± SD. 84 (R-R, Venus), 60 (B-R, Venus), 104 (R-R, cIPAD-1), 55 (B-R, cIPAD-1), 132 (R-R, cIPAD-3), and 107 (B-R, cIPAD-3) cell adhesion sites from three independent experiments were analyzed.

split-GFP technique-based α4 indicator was more than twice as bright as IPAD (Figures 4A and 4B), which will be able to provide a higher signal-to-background ratio. The fact that fluorescence is maintained after EGTA treatment suggests that transient α4 interactions can be recorded as a history (Figures 4C and 4D). In addition, although not addressed by ddGFP, the split-GFP technique is resistant to fixation and immunostaining.[39] Therefore, IPAD and the split-GFP-based α4 indicator can be used for different purposes.

Time-lapse imaging of neurons expressing cIPAD-3 showed that as the processes moved away from each other, the signal was pulled to one of the processes while maintaining its fluorescence, and the fluorescence disappeared after a while (Figure 6F). If the tension between the processes pulls the α4 *trans*-interaction interfaces apart, as it is well illustrated in schematic diagrams, then cIPAD-3 fluorescence should gradually fade as the processes move apart. There are several possibilities that our observational result did not follow this scheme. For example, as Notch receptors are cleaved by a disintegrin and metalloproteinases (ADAMs) due to mechanical forces associated with cell-cell contacts,[52] α4, which is also a substrate of ADAMs,[53,54] may be cleaved by ADAMs, driven by tensions across processes. Alternatively, the α4 *trans*-interacting complex may be unilaterally transferred to one process by a mechanism similar to trogocytosis, a phenomenon observed in immune cells in which receptors are transferred with the membrane from one cell to the other cell upon cell-cell contacts.[55] Or, it may simply be an artifact of cIPAD. A multifaceted approach is needed to clarify how Pcdhs dissociate at the molecular level.

While Pcdhs have been shown to be required for the dendritic self-avoidance in Purkinje cells and starburst amacrine cells,[15–17] it has not been implicated in the self-avoidance in hippocampal neurons. Since we were able to observe static α4 *trans*-interactions by cIPAD, α4 may not be involved in the self-avoidance response of hippocampal neurons (Figures 6C, S6, and S8).

Recently, the detailed process of the dendritic self-avoidance in starburst amacrine cells has been visualized using sophisticated sample preparation and time-lapse imaging.[56,57] Since Pcdhα has been reported to be cooperatively involved with Pcdhγ in the dendritic self-avoidance of starburst amacrine cells,[17] we expect that the combination of cIPAD with the previous sophisticated methods may provide spatiotemporal information on α4 *trans*-interactions in the self-avoidance of starburst amacrine cells in the future. In addition, it is necessary to approach the significance in homophilic interactions of Pcdh by confirming biological functions using IPADs as future effort.

Limitations of the study

We previously reported that ddGFP-based N-cadherin indicators, namely INCIDERs, showed slow decay kinetics upon EGTA treatment, compared to an FRET-based N-cadherin indicator.[43] Since IPADs also use ddGFP, IPADs may show slow decay kinetics upon EGTA treatment.

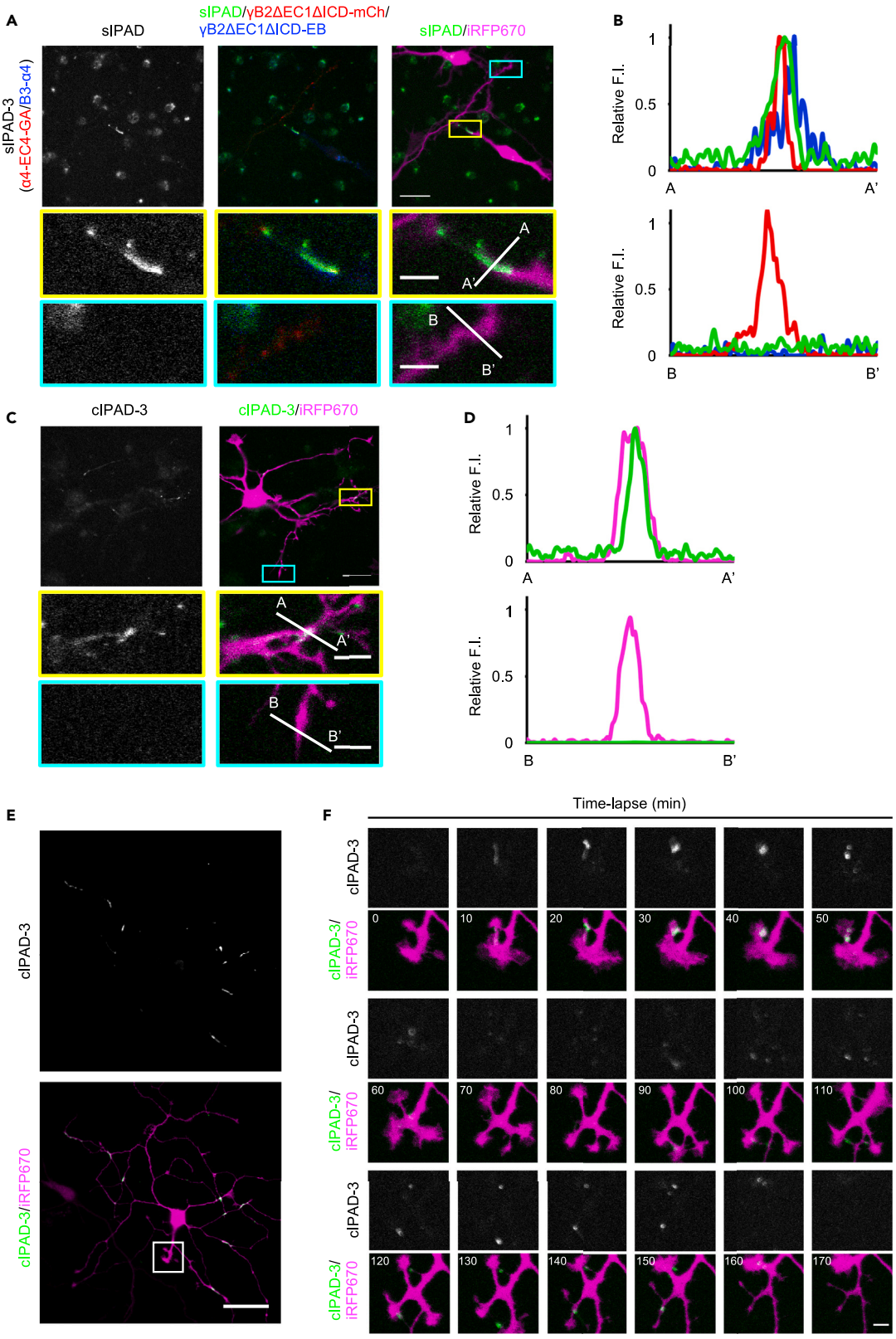
A
sIPAD
sIPAD/γB2ΔEC1ΔICD-mCh/
γB2ΔEC1ΔICD-EB
sIPAD/iRFP670
sIPAD-3
(α4-EC4-GA/B3-α4)
A
A'
B
B'
B
Relative F.I.
1
0.5
0
A
A'
B
B'
C
cIPAD-3
cIPAD-3/iRFP670
D
E
cIPAD-3
cIPAD-3/iRFP670
F
Time-lapse (min)
0
10
20
30
40
50
60
70
80
90
100
110
120
130
140
150
160
170

Figure 6. Visualization of α4 *trans*-interactions in neurons

(A) Fluorescence images of α4 *trans*-interactions in neurons by sIPAD-3. Dissociated hippocampal neurons individually expressing full-length sIPAD-3 components (α4-EC4-GA and B3-α4) were co-cultured and observed using a confocal microscope. γB2ΔEC1ΔICD-mCh and γB2ΔEC1ΔICD-EB were co-expressed with α4-EC4-GA and B3-α4 as carrier proteins, respectively. iRFP670 was co-expressed to visualize cell morphology. Scale bar, 20 μm (upper), 5 μm (lower). Nine fields of view were observed from four independent experiments.

(B) Fluorescence intensities along the white lines across a neuronal process of an α4-EC4-GA-expressing neuron with (from A to A′) or without (from B to B′) a B3-α4-expressing neuron. Relative fluorescence intensities of sIPAD, mCherry, and EBFP2 are indicated by green, red, and blue lines, respectively.

(C) Fluorescence images of α4 *trans*-interactions between processes from a single neuron by cIPAD-3. Dissociated hippocampal neurons expressing cIPAD-3 were observed using a confocal microscope. γB2ΔEC1ΔICD-mCh was co-expressed with cIPAD-3 as a carrier protein. iRFP670 was co-expressed to visualize cell morphology. Scale bar, 20 μm (upper), 5 μm (lower). 25 fields of view were observed from nine independent experiments.

(D) Fluorescence intensities along the white lines across a process of a cIPAD-3- expressing neuron with (from A to A′) or without (from B to B′) a process of the same neuron. Relative fluorescence intensities of cIPAD and iRFP670 are represented by green and magenta lines, respectively.

(E) Dynamics of α4 *trans*-interactions between processes derived from a single neuron. Dissociated hippocampal neurons expressing cIPAD-3 were observed using a confocal microscope. γB2ΔEC1ΔICD-mCh was co-expressed with cIPAD-3 as a carrier protein. iRFP670 was co-expressed to visualize cell morphology. Scale bar, 40 μm. Five neurons were observed from five independent experiments.

(F) Time-lapse images of a cIPAD-3-expressing neuron in a white square region in Figure 6E. Fluorescence images were acquired every 10 min. Scale bar, 5 μm.

IPADs are assumed to function not only as fluorescent indicators, but also as α4. Therefore, it is important to keep in mind that overexpression of IPADs may interfere with endogenous Pcdh functions or disturb the link between Pcdh and intracellular signaling.

Since sIPADs consist of two components, they must be separately introduced into individual cells. In addition, sIPADs seem to be unable to visualize α4 *trans*-interactions between processes originating from the same neurons. In contrast, cIPADs can visualize α4 *trans*-interactions between processes originating from the same neurons. However, cIPADs also visualize α4 *trans*-interactions between different neurons. cIPADs are unable to distinguish process-process interactions from different neurons or from the same neurons under conditions where neurons expressing cIPADs are close to each other. To clearly visualize α4 *trans*-interactions between processes originating from the same cells, cIPADs should be sparsely introduced into neurons.

The coding sequence size of full-length sIPADs components and full-length cIPADs is approximately 3.6 kb and 4.3 kb, respectively. It is possible that their large size may affect the efficiency of gene delivery, such as adeno-associated virus (AAV) methods.

The advantages and limitations of ddGFP-based indicators, including IPADs, compared to indicators based on other techniques are summarized in Table S1.

STAR★METHODS

Detailed methods are provided in the online version of this paper and include the following:

- KEY RESOURCES TABLE
- RESOURCE AVAILABILITY
  - Lead contact
  - Materials availability
  - Data and code availability
- EXPERIMENTAL MODEL AND PARTICIPANT DETAILS
  - Cell culture and plasmid transfection
  - Animals
- METHODS DETAILS
  - Plasmid construction
  - Cell imaging
  - Cell aggregation assay
- QUANTIFICATION AND STATISTICAL ANALYSIS

SUPPLEMENTAL INFORMATION

Supplemental information can be found online at https://doi.org/10.1016/j.isci.2023.107238.

ACKNOWLEDGMENTS

This work was supported by JST PRESTO Program (No. JPMJPR2045) to T.K., JST CREST Program (No. JPMJCR20E4) to T.M., Grant-in-Aid for Scientific Research on Transformative Research Areas (A) Adaptive Circuit Census (No. JP22H05498) to T.Y., and NIH Grant (5R01MH117790-05) to T.Y.

AUTHOR CONTRIBUTIONS

Conceptualization, T.K. and T.Y.; Methodology, T.K.; Formal analysis, T.K.; Investigation, T.K. and N.H.; Writing – Original Draft, T.K.; Writing – Review & Editing, T.K., N.H., T.Y., and T.M.; Supervision, T.K., T.N., T.Y., and T.M.; Project administration, T.K. and T.Y.; Funding acquisition, T.K., T.Y., and T.M.

DECLARATION OF INTERESTS

The authors declare no competing interests.

Received: March 23, 2023
Revised: May 15, 2023
Accepted: June 26, 2023
Published: July 17, 2023

REFERENCES

1. Azevedo, F.A.C., Carvalho, L.R.B., Grinberg, L.T., Farfel, J.M., Ferretti, R.E.L., Leite, R.E.P., Jacob Filho, W., Lent, R., and Herculano-Houzel, S. (2009). Equal numbers of neuronal and nonneuronal cells make the human brain an isometrically scaled-up primate brain. J. Comp. Neurol. *513*, 532–541. https://doi.org/10.1002/cne.21974.

2. Zipursky, S.L., and Grueber, W.B. (2013). The molecular basis of self-avoidance. Annu. Rev. Neurosci. *36*, 547–568. https://doi.org/10.1146/annurev-neuro-062111-150414.

3. Kohmura, N., Senzaki, K., Hamada, S., Kai, N., Yasuda, R., Watanabe, M., Ishii, H., Yasuda, M., Mishina, M., and Yagi, T. (1998). Diversity revealed by a novel family of cadherins expressed in neurons at a synaptic complex. Neuron *20*, 1137–1151. https://doi.org/10.1016/s0896-6273(00)80495-x.

4. Wu, Q., and Maniatis, T. (1999). A striking organization of a large family of human neural cadherin-like cell adhesion genes. Cell *97*, 779–790. https://doi.org/10.1016/s0092-8674(00)80789-8.

5. Esumi, S., Kakazu, N., Taguchi, Y., Hirayama, T., Sasaki, A., Hirabayashi, T., Koide, T., Kitsukawa, T., Hamada, S., and Yagi, T. (2005). Monoallelic yet combinatorial expression of variable exons of the protocadherin-α gene cluster in single neurons. Nat. Genet. *37*, 171–176. https://doi.org/10.1038/ng1500.

6. Kaneko, R., Kato, H., Kawamura, Y., Esumi, S., Hirayama, T., Hirabayashi, T., and Yagi, T. (2006). Allelic gene regulation of *Pcdh-α* and *Pcdh-γ* clusters involving both monoallelic and biallelic expression in single Purkinje cells. J. Biol. Chem. *281*, 30551–30560. https://doi.org/10.1074/jbc.M605677200.

7. Hirano, K., Kaneko, R., Izawa, T., Kawaguchi, M., Kitsukawa, T., and Yagi, T. (2012). Single-neuron diversity generated by protocadherin-β cluster in mouse central and peripheral nervous systems. Front. Mol. Neurosci. *5*, 90. https://doi.org/10.3389/fnmol.2012.00090.

8. Mountoufaris, G., Chen, W.V., Hirabayashi, Y., O'Keeffe, S., Chevee, M., Nwakeze, C.L., Polleux, F., and Maniatis, T. (2017). Multicluster Pcdh diversity is required for mouse olfactory neural circuit assembly. Science *356*, 411–414. https://doi.org/10.1126/science.aai8801.

9. Jia, Z., Li, J., Ge, X., Wu, Y., Guo, Y., and Wu, Q. (2020). Tandem CTCF sites function as insulators to balance spatial chromatin contacts and topological enhancer-promoter selection. Genome Biol. *21*, 75. https://doi.org/10.1186/s13059-020-01984-7.

10. Lv, X., Li, S., Li, J., Yu, X.Y., Ge, X., Li, B., Hu, S., Lin, Y., Zhang, S., Yang, J., et al. (2022). Patterned cPCDH expression regulates the fine organization of the neocortex. Nature *612*, 503–511. https://doi.org/10.1038/s41586-022-05495-2.

11. Schreiner, D., and Weiner, J.A. (2010). Combinatorial homophilic interaction between gamma-protocadherin multimers greatly expands the molecular diversity of cell adhesion. Proc. Natl. Acad. Sci. USA *107*, 14893–14898. https://doi.org/10.1073/pnas.1004526107.

12. Thu, C.A., Chen, W.V., Rubinstein, R., Chevee, M., Wolcott, H.N., Felsovalyi, K.O., Tapia, J.C., Shapiro, L., Honig, B., and Maniatis, T. (2014). Single-cell identity generated by combinatorial homophilic interactions between α, β, and γ protocadherins. Cell *158*, 1045–1059. https://doi.org/10.1016/j.cell.2014.07.012.

13. Rubinstein, R., Goodman, K.M., Maniatis, T., Shapiro, L., and Honig, B. (2017). Structural origins of clustered protocadherin-mediated neuronal barcoding. Semin. Cell Dev. Biol. *69*, 140–150. https://doi.org/10.1016/j.semcdb.2017.07.023.

14. Mountoufaris, G., Canzio, D., Nwakeze, C.L., Chen, W.V., and Maniatis, T. (2018). Writing, reading, and translating the clustered protocadherin cell surface recognition code for neural circuit assembly. Annu. Rev. Cell Dev. Biol. *34*, 471–493. https://doi.org/10.1146/annurev-cellbio-100616-060701.

15. Lefebvre, J.L., Kostadinov, D., Chen, W.V., Maniatis, T., and Sanes, J.R. (2012). Protocadherins mediate dendritic self-avoidance in the mammalian nervous system. Nature *488*, 517–521. https://doi.org/10.1038/nature11305.

16. Kostadinov, D., and Sanes, J.R. (2015). Protocadherin-dependent dendritic self-avoidance regulates neural connectivity and circuit function. Elife *4*, e08964. https://doi.org/10.7554/eLife.08964.

17. Ing-Esteves, S., Kostadinov, D., Marocha, J., Sing, A.D., Joseph, K.S., Laboulaye, M.A., Sanes, J.R., and Lefebvre, J.L. (2018). Combinatorial effects of alpha- and gamma-protocadherins on neuronal survival and dendritic self-avoidance. J. Neurosci. *38*, 2713–2729. https://doi.org/10.1523/JNEUROSCI.3035-17.2018.

18. Hasegawa, S., Hamada, S., Kumode, Y., Esumi, S., Katori, S., Fukuda, E., Uchiyama, Y., Hirabayashi, T., Mombaerts, P., and Yagi, T. (2008). The protocadherin-α family is involved in axonal coalescence of olfactory sensory neurons into glomeruli of the olfactory bulb in mouse. Mol. Cell. Neurosci. *38*, 66–79. https://doi.org/10.1016/j.mcn.2008.01.016.

19. Katori, S., Hamada, S., Noguchi, Y., Fukuda, E., Yamamoto, T., Yamamoto, H., Hasegawa, S., and Yagi, T. (2009). Protocadherin-α family is required for serotonergic projections to appropriately innervate target brain areas. J. Neurosci. *29*, 9137–9147. https://doi.org/10.1523/JNEUROSCI.5478-08.2009.

20. Katori, S., Noguchi-Katori, Y., Okayama, A., Kawamura, Y., Luo, W., Sakimura, K., Hirabayashi, T., Iwasato, T., and Yagi, T. (2017). Protocadherin-αC2 is required for diffuse projections of serotonergic axons. Sci. Rep. *7*, 15908. https://doi.org/10.1038/s41598-017-16120-y.

21. Chen, W.V., Nwakeze, C.L., Denny, C.A., O'Keeffe, S., Rieger, M.A., Mountoufaris, G., Kirner, A., Dougherty, J.D., Hen, R., Wu, Q., and Maniatis, T. (2017). PcdhαC2 is required for axonal tiling and assembly of serotonergic circuitries in mice. Science *356*, 406–411. https://doi.org/10.1126/science.aal3231.

22. Garrett, A.M., Schreiner, D., Lobas, M.A., and Weiner, J.A. (2012). γ-protocadherins control cortical dendrite arborization by regulating the activity of a FAK/PKC/MARCKS signaling pathway. Neuron *74*, 269–276. https://doi.org/10.1016/j.neuron.2012.01.028.

23. Suo, L., Lu, H., Ying, G., Capecchi, M.R., and Wu, Q. (2012). Protocadherin clusters and cell adhesion kinase regulate dendrite complexity through Rho GTPase. J. Mol. Cell Biol. *4*, 362–376. https://doi.org/10.1093/jmcb/mjs034.

24. Molumby, M.J., Keeler, A.B., and Weiner, J.A. (2016). Homophilic protocadherin cell–cell interactions promote dendrite complexity. Cell Rep. *15*, 1037–1050. https://doi.org/10.1016/j.celrep.2016.03.093.

25. Steffen, D.M., Hanes, C.M., Mah, K.M., Valiño Ramos, P., Bosch, P.J., Hinz, D.C., Radley, J.J., Burgess, R.W., Garrett, A.M., and Weiner, J.A. (2023). A unique role for Protocadherin γC3 in promoting dendrite arborization through an Axin1-dependent mechanism. J. Neurosci. *43*, 918–935. https://doi.org/10.1523/JNEUROSCI.0729-22.2022.

26. Molumby, M.J., Anderson, R.M., Newbold, D.J., Koblesky, N.K., Garrett, A.M., Schreiner, D., Radley, J.J., and Weiner, J.A. (2017). γ-protocadherins interact with neuroligin-1 and negatively regulate dendritic spine morphogenesis. Cell Rep. *18*, 2702–2714. https://doi.org/10.1016/j.celrep.2017.02.060.

27. Steffen, D.M., Ferri, S.L., Marcucci, C.G., Blocklinger, K.L., Molumby, M.J., Abel, T., and Weiner, J.A. (2021). The γ-protocadherins interact physically and functionally with neuroligin-2 to negatively regulate inhibitory synapse density and are required for normal social interaction. Mol. Neurobiol. *58*, 2574–2589. https://doi.org/10.1007/s12035-020-02263-z.

28. Fan, L., Lu, Y., Shen, X., Shao, H., Suo, L., and Wu, Q. (2018). Alpha protocadherins and Pyk2 kinase regulate cortical neuron migration and cytoskeletal dynamics via Rac1 GTPase and WAVE complex in mice. Elife *7*, e35242. https://doi.org/10.7554/eLife.35242.

29. Wang, X., Weiner, J.A., Levi, S., Craig, A.M., Bradley, A., and Sanes, J.R. (2002). Gamma protocadherins are required for survival of spinal interneurons. Neuron *36*, 843–854. https://doi.org/10.1016/s0896-6273(02)01090-5.

30. Lefebvre, J.L., Zhang, Y., Meister, M., Wang, X., and Sanes, J.R. (2008). gamma-Protocadherins regulate neuronal survival but are dispensable for circuit formation in retina. Development *135*, 4141–4151. https://doi.org/10.1242/dev.027912.

31. Chen, W.V., Alvarez, F.J., Lefebvre, J.L., Friedman, B., Nwakeze, C., Geiman, E., Smith, C., Thu, C.A., Tapia, J.C., Tasic, B., et al. (2012). Functional significance of isoform diversification in the protocadherin gamma gene cluster. Neuron *75*, 402–409. https://doi.org/10.1016/j.neuron.2012.06.039.

32. Garrett, A.M., Bosch, P.J., Steffen, D.M., Fuller, L.C., Marcucci, C.G., Koch, A.A., Bais, P., Weiner, J.A., and Burgess, R.W. (2019). CRISPR/Cas9 interrogation of the mouse Pcdhg gene cluster reveals a crucial isoform-specific role for PcdhgC4. PLoS Genet. *15*, e1008554. https://doi.org/10.1371/journal.pgen.1008554.

33. Mancia Leon, W.R., Spatazza, J., Rakela, B., Chatterjee, A., Pande, V., Maniatis, T., Hasenstaub, A.R., Stryker, M.P., and Alvarez-Buylla, A. (2020). Clustered gamma-protocadherins regulate cortical interneuron programmed cell death. Elife *9*, e55374. https://doi.org/10.7554/eLife.55374.

34. Kobayashi, H., Takemoto, K., Sanbo, M., Hirabayashi, M., Hirabayashi, T., Hirayama, T., Kiyonari, H., Abe, T., and Yagi, T. (2023). Isoform requirement of clustered protocadherin for preventing neuronal apoptosis and neonatal lethality. iScience *26*, 105766. https://doi.org/10.1016/j.isci.2022.105766.

35. Kerppola, T.K. (2006). Visualization of molecular interactions by fluorescence complementation. Nat. Rev. Mol. Cell Biol. *7*, 449–456. https://doi.org/10.1038/nrm1929.

36. Shyu, Y.J., and Hu, C.D. (2008). Fluorescence complementation: an emerging tool for biological research. Trends Biotechnol. *26*, 622–630. https://doi.org/10.1016/j.tibtech.2008.07.006.

37. Feinberg, E.H., Vanhoven, M.K., Bendesky, A., Wang, G., Fetter, R.D., Shen, K., and Bargmann, C.I. (2008). GFP Reconstitution Across Synaptic Partners (GRASP) defines cell contacts and synapses in living nervous systems. Neuron *57*, 353–363. https://doi.org/10.1016/j.neuron.2007.11.030.

38. Kim, J., Zhao, T., Petralia, R.S., Yu, Y., Peng, H., Myers, E., and Magee, J.C. (2012). mGRASP enables mapping mammalian synaptic connectivity with light microscopy. Nat. Methods *9*, 96–102. https://doi.org/10.1038/nmeth.1784.

39. Tsetsenis, T., Boucard, A.A., Araç, D., Brunger, A.T., and Südhof, T.C. (2014). Direct visualization of trans-synaptic neurexin-neuroligin interactions during synapse formation. J. Neurosci. *34*, 15083–15096. https://doi.org/10.1523/JNEUROSCI.0348-14.2014.

40. Choi, J.H., Sim, S.E., Kim, J.I., Choi, D.I., Oh, J., Ye, S., Lee, J., Kim, T., Ko, H.G., Lim, C.S., and Kaang, B.K. (2018). Interregional synaptic maps among engram cells underlie memory formation. Science *360*, 430–435. https://doi.org/10.1126/science.aas9204.

41. Kinoshita, N., Huang, A.J.Y., McHugh, T.J., Suzuki, S.C., Masai, I., Kim, I.H., Soderling, S.H., Miyawaki, A., and Shimogori, T. (2019). Genetically encoded fluorescent indicator GRAPHIC delineates intercellular connections. iScience *15*, 28–38. https://doi.org/10.1016/j.isci.2019.04.013.

42. Kinoshita, N., Huang, A.J.Y., McHugh, T.J., Miyawaki, A., and Shimogori, T. (2020). Diffusible GRAPHIC to visualize morphology of cells after specific cell–cell contact. Sci. Rep. *10*, 14437. https://doi.org/10.1038/s41598-020-71474-0.

43. Kanadome, T., Hayashi, K., Seto, Y., Eiraku, M., Nakajima, K., Nagai, T., and Matsuda, T. (2022). Development of intensiometric indicators for visualizing N-cadherin interaction across cells. Commun. Biol. *5*, 1065. https://doi.org/10.1038/s42003-022-04023-2.

44. Alford, S.C., Ding, Y., Simmen, T., and Campbell, R.E. (2012). Dimerization-dependent green and yellow fluorescent proteins. ACS Synth. Biol. *1*, 569–575. https://doi.org/10.1021/sb300050j.

45. Ding, Y., Li, J., Enterina, J.R., Shen, Y., Zhang, I., Tewson, P.H., Mo, G.C.H., Zhang, J., Quinn, A.M., Hughes, T.E., et al. (2015). Ratiometric biosensors based on dimerization-dependent fluorescent protein exchange. Nat. Methods *12*, 195–198. https://doi.org/10.1038/nmeth.3261.

46. Murata, Y., Hamada, S., Morishita, H., Mutoh, T., and Yagi, T. (2004). Interaction with protocadherin-gamma regulates the cell surface expression of protocadherin-alpha. J. Biol. Chem. *279*, 49508–49516. https://doi.org/10.1074/jbc.M408771200.

47. Goodman, K.M., Rubinstein, R., Dan, H., Bahna, F., Mannepalli, S., Ahlsén, G., Aye Thu, C., Sampogna, R.V., Maniatis, T., Honig, B., and Shapiro, L. (2017). Protocadherin *cis*-dimer architecture and recognition unit diversity. Proc. Natl. Acad. Sci. USA *114*, E9829–E9837. https://doi.org/10.1073/pnas.1713449114.

48. Fernández-Monreal, M., Kang, S., and Phillips, G.R. (2009). Gamma-protocadherin homophilic interaction and intracellular trafficking is controlled by the cytoplasmic domain in neurons. Mol. Cell. Neurosci. *40*, 344–353. https://doi.org/10.1016/j.mcn.2008.12.002.

49. Kanadome, T., Hoshino, N., Nagai, T., Matsuda, T., and Yagi, T. (2021). Development of FRET-based indicators for visualizing homophilic *trans* interaction of a clustered protocadherin. Sci. Rep. *11*, 22237. https://doi.org/10.1038/s41598-021-01481-2.

50. Goodman, K.M., Rubinstein, R., Thu, C.A., Bahna, F., Mannepalli, S., Ahlsén, G., Rittenhouse, C., Maniatis, T., Honig, B., and Shapiro, L. (2016). Structural Basis of Diverse Homophilic Recognition by Clustered α- and β-Protocadherins. Neuron *90*, 709–723.

https://doi.org/10.1016/j.neuron.2016.04.004.

51. Ozawa, M., and Kemler, R. (1998). Altered cell adhesion activity by pervanadate due to the dissociation of α-catenin from the E-cadherin.catenin complex. J. Biol. Chem. *273*, 6166–6170. https://doi.org/10.1074/jbc.273.11.6166.

52. Gordon, W.R., Zimmerman, B., He, L., Miles, L.J., Huang, J., Tiyanont, K., McArthur, D.G., Aster, J.C., Perrimon, N., Loparo, J.J., and Blacklow, S.C. (2015). Mechanical Allostery: Evidence for a Force Requirement in the Proteolytic Activation of Notch. Dev. Cell *33*, 729–736. https://doi.org/10.1016/j.devcel.2015.05.004.

53. Bonn, S., Seeburg, P.H., and Schwarz, M.K. (2007). Combinatorial expression of α- and γ-protocadherins alters their presenilin-dependent processing. Mol. Cell Biol. *27*, 4121–4132. https://doi.org/10.1128/MCB.01708-06.

54. Buchanan, S.M., Schalm, S.S., and Maniatis, T. (2010). Proteolytic processing of protocadherin proteins requires endocytosis. Proc. Natl. Acad. Sci. USA *107*, 17774–17779. https://doi.org/10.1073/pnas.1013105107.

55. Ahmed, K.A., Munegowda, M.A., Xie, Y., and Xiang, J. (2008). Intercellular trogocytosis plays an important role in modulation of immune responses. Cell. Mol. Immunol. *5*, 261–269. https://doi.org/10.1038/cmi.2008.32.

56. Ing-Esteves, S., and Lefebvre, J.L. (2022). Gamma-Protocadherins regulate filopodia self-recognition and dynamics to drive dendrite self-avoidance. Preprint at bioRxiv. https://doi.org/10.1101/2022.11.23.517768.

57. Ing-Esteves, S., and Lefebvre, J.L. (2021). Time-Lapse Imaging of Neuronal Arborization using Sparse Adeno-Associated Virus Labeling of Genetically Targeted Retinal Cell Populations. J. Vis. Exp. *169*. https://doi.org/10.3791/62308.

58. Schneider, C.A., Rasband, W.S., and Eliceiri, K.W. (2012). NIH Image to ImageJ: 25 years of image analysis. Nat. Methods *9*, 671–675. https://doi.org/10.1038/nmeth.2089.

STAR★METHODS

KEY RESOURCES TABLE

REAGENT or RESOURCE	SOURCE	IDENTIFIER
Bacterial and virus strains		
Escherichia coli strain XL10-Gold	Agilent Technologies	Cat#200314
Chemicals, peptides, and recombinant proteins		
NheI	Takara	Cat#1241A
BsrGI	New England Biolabs	Cat#R0575S
AgeI	Nippon Gene	Cat#313-02561
BglII	Takara	Cat#1021A
Dulbecco's modified Eagle's medium	Sigma-Aldrich	Cat#D6046
Fetal bovine serum	Biowest	N/A
Fetal bovine serum	ThermoFisher Scientific	N/A
Iscove's modified Dulbecco's medium	ThermoFisher Scientific	Cat#12440053
Polyethylenimine "MAX"	Cosmo Bio	Cat#24765-1
Neuron Dissociation Solutions	Wako	Cat#291-78001
Minimum essential media	ThermoFisher Scientific	Cat#11090-081
FluoroBrite DMEM	ThermoFisher Scientific	Cat#A1896701
B-27 supplement	ThermoFisher Scientific	Cat#17504044
GlutaMAX	ThermoFisher Scientific	Cat#35050061
Penicillin-Streptomycin (10,000 U/mL)	ThermoFisher Scientific	Cat#15140122
HEPES (1 M)	ThermoFisher Scientific	Cat#15630080
Poly-L-lysine hydrobromide	Sigma-Aldrich	Cat#P2636
Cytosine β-D-arabinofuranoside hydrochloride	Sigma-Aldrich	Cat#C6645
Trypsin-EDTA (0.25%) and phenol red	ThermoFisher Scientific	Cat#25200072
DMEM/F12, HEPES, no phenol red	ThermoFisher Scientific	Cat#11039-021
Polyethylenimine	Sigma-Aldrich	Cat#P3143
IMDM, no phenol red	ThermoFisher Scientific	Cat#21056023
Experimental models: Cell lines		
HEK293T	RIKEN BRC	N/A
K562	RIKEN BRC	N/A
Experimental models: Organisms/strains		
Mouse: C57/B6J	Japan SLC	N/A
Recombinant DNA		
pCX:α4ΔICD-V	This paper	N/A
pCX:V-α4ΔICD	This paper	N/A
pCX:α4ΔICD-EC4-V	This paper	N/A
pCX:α4ΔICD-EC4-GA	This paper	N/A
pCX:α4-EC4-GA	This paper	N/A
pCX:B1-α4ΔICD	This paper	N/A
pCX:B1-α4	This paper	N/A
pCX:B3-α4ΔICD	This paper	N/A
pCX:B1-α4	This paper	N/A
pCX:γB2ΔICD-mCh	This paper	N/A

(*Continued on next page*)

Continued

REAGENT or RESOURCE	SOURCE	IDENTIFIER
pCX:γB2ΔICD-EB	This paper	N/A
pCX:γB2ΔEC1ΔICD-mCh	This paper	N/A
pCX:γB2ΔEC1ΔICD-EB	This paper	N/A
pCX:α8ΔICD-EC4-GA	This paper	N/A
pCX:B1-α8ΔICD	This paper	N/A
pCX:B3-α8ΔICD	This paper	N/A
pCX:γA3ΔICD-mCh	This paper	N/A
pCX:γA3ΔICD-EB	This paper	N/A
pCX:α4ΔICD-EC4-sfGN	This paper	N/A
pCX:sfGC-α4ΔICD	This paper	N/A
pCX:cIPAD-1 (ΔICD)	This paper	N/A
pCX:cIPAD-1 (full length)	This paper	N/A
pCX:cIPAD-3 (ΔICD)	This paper	N/A
pCX:cIPAD-3 (full length)	This paper	N/A
pCAGGS1:mCh-NLS	Kanadome et al.,[43]	N/A
pCX:iRFP670	This paper	N/A
pCX:γB2ΔICD-V	Kanadome et al.,[49]	N/A
pCX:α4γB2EC6ΔICD-V	This paper	N/A
pCX:α4γB2EC6ΔICD-EC1-V	This paper	N/A
pCX:α4γB2EC6ΔICD-EC5-V	This paper	N/A
pCX:V-α4γB2EC6ΔICD	This paper	N/A
pCX:α4γB2EC6ΔICD-EC4-V	This paper	N/A
Software and algorithms		
GraphPad Prism9	GraphPad Software, Inc.	https://www.graphpad.com/; RRID:SCR_002798
ImageJ (FIJI)	Schneider et al.,[58]	https://imagej.nih.gov/ij/; RRID:SCR_002285

RESOURCE AVAILABILITY

Lead contact

Further information and requests for resources and reagents should be directed to and will be fulfilled by the lead contact, Takashi Kanadome (tk4@sanken.osaka-u.ac.jp).

Materials availability

Plasmids generated in this study are available from the authors on reasonable request.

Data and code availability

- Data reported in this paper will be shared by the lead contact upon request.
- This paper does not report original code.
- Any additional information required for data reported in this paper is available from the lead contact upon reasonable request.

EXPERIMENTAL MODEL AND PARTICIPANT DETAILS

Cell culture and plasmid transfection

HEK293T cells (RIKEN BRC) were maintained in Dulbecco's modified Eagle's medium (DMEM, Sigma-Aldrich) supplemented with 10% (v/v) fetal bovine serum (FBS, Biowest) at 37°C in humidified air containing 5% CO_2. K562 (RIKEN BRC) cells were maintained in Iscove's modified Dulbecco's medium (IMDM, Thermo Fisher Scientific) supplemented with 10% (v/v) FBS.

HEK293T cells were transfected using polyethylenimine MAX (Cosmo Bio). K562 cells were electroporated using an electroporator (NEPA21: NEPAGENE) with the following conditions: 1 × 10^6 dissociated cells, 10 μg of plasmid, porting pulse (275 V, 1 ms pulse length, 50 ms interval, twice, 10% decay rate), and transfer pulse (20 V, 50 ms pulse length, 50 ms interval, 5 times, 40% decay rate).

For primary culture of hippocampal neurons, hippocampi were collected from E18 embryos (C57/B6J) and were digested with Neuron Dissociation Solutions (Wako) according to the manufacturer's protocol. Minimum essential Media (MEM, ThermoFisher Scientific) or FluoroBrite DMEM (ThermoFisher Scientific) were supplemented with 5.5% FBS (ThermoFisher Scientific), 2% B27 supplement (ThermoFisher Scientific), 1 mM GlutaMAX (ThermoFisher Scientific), 100 units/mL Penicillin-100 μg/mL streptomycin (ThermoFisher Scientific), and 10 mM HEPES (1 M) (Gibco). The dissociated cells were washed in a MEM-based medium. The cells were then electroporated using an Amaxa 4D-Nucleofector (Lonza). The transfected cells were suspended in a MEM-based medium and plated on a poly L-lysine (Sigma-Aldrich) treated CELLview glass bottom dish (Advanced TC, 4-compartments) (Greiner). After 2 h, the medium was replaced with the FluoroBrite DMEM-based medium. The following day, 5 mM cytosine β-D-arabinofuranoside hydrochloride (Sigma-Aldrich) was added to a final concentration of 5 nM. The cells were incubated at 37°C in humidified air containing 5% CO_2, without any medium changes.

Animals

Animal experimentation was performed according to the Institutional Guidelines on Animal Experimentation at Osaka University (approval number: FBS-22-008).

METHODS DETAILS

Plasmid construction

All expression plasmids were subcloned into a pCX vector. Monomeric Venus (A206K) was used for the following constructions and will be referred to as Venus. The amino acid positions of α4 are described in the immature form in this section. To generate full-length V-α4 and α4-EC4-V, we inserted Venus flanked by NheI sites at amino acid position 29 between a prodomain and an EC1 domain, and at amino acid position 393 in an EC4 domain of α4 tagged with the HA tag, respectively by overlapping PCR. α4ΔICD constructs were created by deletion of ICD (745–947 amino acids). sIPAD (-1 or -3) without ICD, α4ΔICD-EC4-GA and B (1 or 3)-α4ΔICD were generated by insertion of ddGFP-A and ddFP-B (1 or 3) flanked by NheI sites into α4ΔICD-EC4-V and V-α4ΔICD, respectively. Split-GFP constructs, α4ΔICD-EC4-sfGN and sfGC-α4ΔICD, were constructed by inserting an N-terminus of superfolder GFP (1-159 amino acids) and a C-terminus of superfolder GFP (160-238 amino acids) into α4ΔICD-EC4-GA and B1-α4ΔICD that ddFPs were excised by NheI, respectively. cIPAD (-1 or -3) lacking an ICD were constructed by inserting a product obtained by digestion of α4ΔICD-EC4-GA with BsrGI into B (1 or 3)-α4ΔICD. Full-length cIPAD (-1 or -3) were prepared by inserting an ICD obtained by digestion of full-length α4 with AgeI and BglII into AgeI- and BglII-digested sIPAD (-1 or -3).

Cell imaging

HEK293T cells grown on glass-bottomed dishes coated with Cellmatrix Type I-C (Nitta gelatin) were transiently transfected with expression plasmids and incubated overnight. Before imaging, the medium was replaced with phenol red-free DMEM/F12 (Thermo Fisher Scientific). Fluorescence and DIC images were acquired using an Olympus FV-1000 laser scanning confocal microscope with an IX81 microscope equipped with a x60, 1.35 numerical aperture (NA) oil-immersion objective lens (UPLSAPO60XO) (Olympus). The excitation wavelengths for EBFP2, IPAD, Venus, mCherry, and miRFP670 were 405, 488, 488, 543, and 633 nm, respectively. For co-culture experiments, HEK293T cells were individually transfected with expression plasmids and incubated overnight. The cells were detached from the dishes using trypsin-EDTA (0.25%) and phenol red (Thermo Fisher Scientific) and mixed in 10% FBS/DMEM. Imaging was performed after 24 h. For co-culture experiments to compare between IPAD and split-GFP (Figure 4), HEK293T cells were individually transfected with expression plasmids and cultured for 24 h. The cells were then washed with PBS containing 1 mM EDTA and mixed in phenol red-free DMEM/F12 supplemented with 10% FBS and 100 U/mL Penicillin-Streptomycin (Thermo Fisher Scientific). Cells were co-cultured in a 15-mL conical tube under slow rotation at room temperature for 8 h and seeded onto a glass-bottomed dish coated with 0.1% (w/v) polyethylenimine (P3143, Sigma-Aldrich).

Primary cultures of hippocampal neurons were observed at days *in vitro* (DIV) 2–7. Fluorescence and DIC images were acquired using an LSM780 laser scanning confocal microscope with a x40, 1.4 NA oil-immersion objective lens (Plan-Apochromat 40x/1.4 Oil DIC M27) (Zeiss). The excitation wavelengths for EBFP2, IPAD, mCherry, and iRFP670 were 405, 488, 561, and 633 nm, respectively.

Cell aggregation assay

Cell aggregation assay using K562 cells was performed as described previously.[43] Transfected K562 cells were cultured in IMDM, no phenol red (Thermo Fisher Scientific) supplemented with 10% FBS and 100 U/mL Penicillin-Streptomycin under rotation at 30 rpm overnight at 37°C in humidified air containing 5% CO_2. Before imaging, cells were transferred by decantation to glass-bottomed dishes coated with 0.1% (w/v) polyethylenimine (P3143, Sigma-Aldrich) and incubated for 1 h at 37°C in humidified air containing 5% CO_2.

QUANTIFICATION AND STATISTICAL ANALYSIS

Statistical analyses were performed using GraphPad Prism 9 (GraphPad Software, Inc.). Kolmogorov-Smirnov test was performed for analyses in Figures 2C, 4D, 5C, and 5E. Kruskal-Wallis test, followed by Dunn's multiple comparison test was performed for analyses in Figures 1E, 2E, 3B, 3D, and 4B p values < 0.05 were considered statistically significant. Data in Figures 1E, 2C, 2E, 3B, 3D, 4B, 5C, and 5E are shown as lower quartile (lower whisker), median (center line), and upper quartile (upper whisker). Data in Figures 4D and 5H are shown as mean ± SD. Sample sizes are listed in the Figure legends for each experiment. Reproducibility was confirmed by at least two independent experiments.